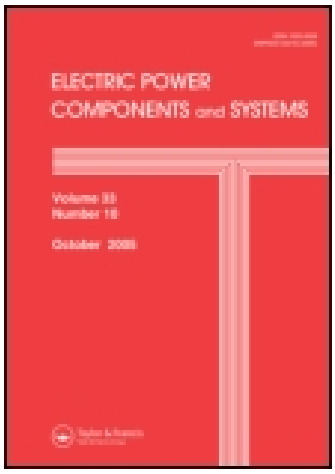

Electric Power Components and Systems

Publication details, including instructions for authors and subscription information:
http://www.tandfonline.com/loi/uemp20

Flicker Source Tracing by Wavelet Transform

Hadi Moghadam Banayem[a], Aref Doroudi[a] & Mohammad Poormonfared Azimi[a]

[a] Department of Electrical of Engineering, Shahed University, Tehran, Iran

Published online: 09 Feb 2015.

Electric Power Components and Systems, 43(4):412–421, 2015

ISSN: 1532-5008 print / 1532-5016 online
DOI: 10.1080/15325008.2014.987334

Taylor & Francis
Taylor & Francis Group

Flicker Source Tracing by Wavelet Transform

Hadi Moghadam Banayem, Aref Doroudi, and Mohammad Poormonfared Azimi
Department of Electrical of Engineering, Shahed University, Tehran, Iran

CONTENTS

Abstract—In the present day, voltage fluctuations (flicker) have received more attention by both utilities and consumers. Flicker mitigation needs identification of the flicker sources. After identifying the flicker sources, it would also be possible to penalize the relevant utility or the consumers. In this article, a new method based on flicker power theory and wavelet transform is proposed to identify the locations of single and multiple flicker sources in a multi-flicker source power network. The wavelet transform is utilized for demodulation and then the total flicker powers are computed by adding the flicker power belongs to individual flicker frequency components. The method also computes the contributions of each consumer and utility to the global flicker level of a common coupling busbar. For validation, the IEEE 13-bus network is simulated and an algorithm for flicker sources tracing is tested. Time-domain simulations in MATLAB/Simulink (The MathWorks, Natick, Massachusetts, USA) are performed to examine the accuracy of the proposed method. Simulation results show that by using the proposed method, all flicker sources and their contributions on the global flicker level can be detected correctly. To assess the performance of the proposed algorithm, the comparison with the most well-known methods has been presented.

1. INTRODUCTION

Currently, utilities try their best to provide high-quality power supply for their consumers. However, for various reasons the consumers occasionally encounter unexpected irregularities in their power supply which may cause equipment failure and malfunction. Power quality has, therefore, become an increasing concern for both utilities and consumers.

Due to repeated accidents and customers' complaints, voltage fluctuations or flicker problems have currently received more attention [1].Voltage flicker is referred to the periodical or stochastic changes of voltage waveform which originates from heavy loads such as motors, arc furnaces, rolling mills, welding machines, etc. [2–4]. Wind farms may also produce voltage fluctuations [5, 6].

Generally, according to IEC 61 000-4-15 [7], when voltage fluctuations exceed certain magnitude (up to $\pm 10\%$) for certain repetition frequencies (0.5 to 35 Hz), this phenomenon is observed as a disturbing unsteadiness of the light intensity by human eyes. The fluctuations have a direct impact on light flicker [8]. Moreover, this phenomenon causes some noises

Keywords: power quality, voltage fluctuations, flicker source identification, flicker power, wavelet transform, flicker contributions
Received 14 October 2013; accepted 28 October 2014
Address correspondence to Aref Doroudi, Department of Electrical Engineering, Shahed University, Tehran-Quam Highway, Tehran, 3319118651, Iran. E-mail: doroudi@shahed.ac.ir

NOMENCLATURE

f_b	= network frequency	$m_i(t)$	= envelopes or low-frequency fluctuations of $i(t)$
f_h	= maximum of network frequency	$m\prime_i(t)$	= filtered $m_i(t)$ by IEC 61000-4-15
f_l	= minimum of network frequency	$m_u(t)$	= envelopes or low-frequency fluctuations of $u(t)$
f_m	= flicker mth component frequency	$m\prime_u(t)$	= filtered $m_u(t)$ by IEC 61000-4-15
$FP(t)$	= instantaneous flicker power	T_s	= sampling interval
f_{ru}	= network frequency resolution	$u(t)$	= measured signals of voltage at monitoring point
f_{rf}	= flicker frequency resolution	u_m	= flicker mth component amplitude
f_s	= sampling frequency	$\lambda(t)$	= wavelet function
$i(t)$	= measured signals of current at monitoring point		

in TV sets, malfunction of phase-locked loops, and incorrect operation of clinical equipment, such as electrocardiogram (ECG) used in intensive care unit (ICU) and critical care unit (CCU) systems (this equipment may present different reports of the patients depending on different amplitudes of supplied voltage).

So far, different measurement methods have been proposed to quantify the voltage flicker level. The most comprehensive method has been presented in IEC 61000-4-15, where the values of short-term (P_{st}) and long-term (P_{lt}) flicker levels are measured. However, both levels provide the flicker amount at the monitoring point without any information about the flicker direction in power network. In addition, these quantities are not able to identify the dominant flicker source. Detecting the flicker sources is the first step to mitigate flicker. Identification of flicker sources is of great interest to both utilities and customers.

Within this topic, some research has been presented in the literature that is not based on IEC 61000-4-15 [9–15]. The method proposed in [16, 17] was an analytical approach to determine the direction of flicker source with respect to monitoring point in the same way defined in the IEC standard. Both articles are based on a new quantity called "flicker power" (FP), which is defined as integration of the product of voltage envelopes and current amplitude modulating signals. The envelopes of the modulating signals are recovered by demodulation and passed through some suitable filters. The sign of the FP is applied to determine the direction of a flicker source. A positive sign indicates an upstream flicker source, whereas a negative sign of the FP shows a downstream flicker source with respect to a monitoring point. A disadvantage of both methods presented in [16, 17] is that they used conventional demodulators such as square and envelope detectors, which generate additional low-frequency components in flicker frequency window that makes them impossible to superpose FP correctly. In [18], a novel algorithm based on coherent detector was proposed to improve the method presented in [16, 17].

On the other hand, finding a dominant flicker source is an important issue when there are multiple flicker sources in a common power grid. Once a flicker problem arises, the utility provider will face complaints and even requirements for mitigation from consumers. As a result, the utility provider wants to be perfectly sure that they are discussing with the customer whose equipment has caused the flicker, and consumers want to be convinced that they are the actual polluters of flicker and the main cause of the problem. Any disagreement about the flicker source would slow down the process of mitigation. After identifying the flicker sources, it would be possible to penalize the relevant utility or the consumers. The previous methods specify just a single value for FP at a monitoring point, and therefore, only the dominant flicker source can be identified. The methods are thus not able to determine the locations and contributions of each flicker source in a multi-flicker source power network.

Wavelet transform (WT) has been widely used in distinguishing feature extraction of power quality events and disturbance classification [19, 20]. Angrisani *et al.* [19] proposed an approach for estimating of magnitudes and durations of disturbances using continuous WT and used these two features for identifying voltage sags. To have a better joint time-frequency representation, Hasheminejad *et al.* [20] used a modified WT (S-transform), which provides a time frequency representation with a frequency-dependent resolution, while simultaneously time maintaining the direct relationship, through time-averaging, with the Fourier spectrum. The power quality disturbance signals are sag, swell, harmonic, oscillatory transient, flicker, and the combination of either sag and harmonic or swell and harmonic. The identification procedure has two major steps. First, features are extracted by S-transform, and in the second step, classification is done using a decision tree structure of hidden Markov models.

In this article, a novel method, which is based on WT as demodulator, has been proposed to identify the number and locations of flicker sources in a multi-flicker source power

grid. The method also computes the contributions of individual consumers and utility providers in the global flicker level of a common coupling busbar. A discrete version of a continuous WT is applied to decompose the flicker signal into several flicker frequency components with known amplitude and phase angles. Then, the proposed method finds out the total FP and FP at each flicker frequency component individually. The method is such that superposition principle can be applied. With defining the FP at each flicker frequency as a quantity which contains both the sign and the magnitude, the problem could be solved.

The article is organized as follows: A brief introduction to FP theory and flicker modeling are discussed in Sections 2 and 3. In Section 4, the proposed method is introduced. Simulations results in a test network are given in Section 5, and finally in Section 6, conclusions are drawn.

2. FP THEORY

The FP theory is based on the following facts [16]:

- A flicker source causes changes in the envelopes of both voltage and current signals (amplitude modulation) at the monitoring point.
- Changes in voltage and current are in phase if the flow direction of flicker is upstream and 180 degrees out of phase if the flicker source is located below (downstream) to a monitoring point.

If voltage and current signals being amplitude modulated (AM), they can be expressed as:

$$\begin{aligned} u(t) &= [U_m + m_u(t)]\mathrm{Cos}(\omega_s t + \alpha), \\ i(t) &= [I_m + m_i(t)]\mathrm{Cos}(\omega_s t + \beta), \end{aligned} \tag{1}$$

where $U_m\mathrm{Cos}(\omega_s t + \alpha)$ and $I_m\mathrm{Cos}(\omega_s t + \beta)$ represent fundamental components of voltage and current signals, respectively. The envelopes or low-frequency fluctuations are represented by $m_u(t)$ and $m_i(t)$. The instantaneous $FP(t)$ is thus defined as

$$FP(t) = m_u^{'}(t).m_i^{'}(t) \tag{2}$$

where $m'_u(t)$ and $m'_i(t)$ are obtained from $m_u(t)$ and $m_i(t)$ using the sensitivity filter presented in IEC 61000-4-15.

FP is expressed as

$$FP = \frac{1}{T}\int_{t}^{t+T} m_u^{'}(\tau).m_i^{'}(\tau)d\tau, \tag{3}$$

where T is the time of integration, which was selected as 2 sec in [16, 17]. A positive sign of FP indicates an upstream flicker source while the negative sign indicates downstream flicker source with respect to a monitoring point.

3. FLICKER MODELING

Voltage fluctuating (flicker) is caused by heavy fluctuating loads. Due to the load characteristics its behaviors may be different. Nevertheless, in a short period, the voltage flicker can be approached by an amplitude modulation formula [22]. With this assumption, voltage flicker can be expressed as follows:

$$\begin{aligned} u(t) &= \sqrt{2}[U_s + \sum_m U_m \sin(2\pi f_m t + \alpha_m)].\cos(2\pi f_b t + \alpha) \\ &= \sqrt{2}U_s \cos(2\pi f_b t + \alpha) + \sum_m \frac{U_m}{\sqrt{2}}\sin[2\pi(f_b - f_m)t, \\ &\quad +\alpha_m^-] + \sum_m \frac{U_m}{\sqrt{2}}\sin[2\pi(f_b + f_m)t + \alpha_m^+] \end{aligned} \tag{4}$$

where

U_s is the reference root-mean-square (RMS) value of the network signal without flicker,
f_b is the network frequency,
f_m is the flicker mth component (flicker demodulation) frequency,
U_m is the flicker mth component amplitude (flicker modulation depth) at f_m,
α and α_m are the fundamental signal and the flicker mth component phase angles, respectively.

Figure 1 shows a simplified voltage flicker waveform and its envelope in which the voltage flicker is composed of two modulation voltages $\frac{U_1}{\sqrt{2}} = \frac{U_2}{\sqrt{2}} = 10$V and two modulation frequencies $f_1 = 10$ Hz and $f_2 = 20$ Hz. The network frequency is 50 Hz.

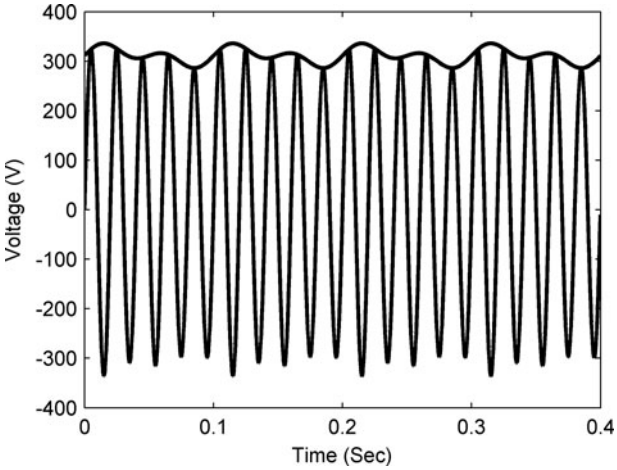

FIGURE 1. Simplified voltage flicker waveform.

4. DESCRIPTION OF THE PROPOSED METHOD

Identification of flicker sources is an important issue when multiple flicker sources are present in the same power network grid. In the previous methods within this topic, only the dominant flicker source has been considered and the methods do not include any information about the number, locations, and contributions of the individual flicker sources in a multi-flicker source network. In this article, a novel algorithm based on FP theory and WT is proposed, which is able to locate the flicker sources individually. Moreover, the proposed method can specify the flicker contributions of the branches that are linked to the same busbar. The block diagram of the proposed algorithm has been shown in Figure 2.

The input signals, $u[n]$ and $i[n]$, are sample versions of the measured analog signals of the voltage and current at the monitoring point. The interface module consists of voltage and current transducers, low pass filter, and an analog-to-digital (A/D) converter [16, 21]. Blocks 1A/1B perform the demodulation process with the WT. The outputs of these blocks are all low-frequency fluctuations (envelopes) modulated to the input signals which are extracted from the base signal and separated from each other according to their frequency (flicker frequency). The individual signals that are characterized by amplitude (depth), frequency, and phase angle are then filtered according to the way that human responds to flicker in blocks 2A/2B. The band-pass filter in these blocks is the sensitivity filter with the transfer function described in IEC 61000-4-15. The filtered signals (outputs of the blocks 2A/2B) indicate how a typical person responds to flicker. Finally, the FPs are computed at the block 3 for all individual flicker frequencies. The FP at each flicker frequency is a quantity which contains both the sign and the magnitude. If the sign of the FP is positive, it means that the flicker source is located upstream while the negative sign indicates a downstream flicker source with respect to a monitoring point [16, 17]. On the other hand, the magnitude of FPs shows the degree of correlation between the envelopes of the current and voltage signals. This implies that by calculating the FP magnitude on several branches that are linked to the same busbar, branch contribution to the busbar flicker level can be determined. Bigger magnitude contributes more to the global flicker level. The details of the blocks will be described in the following text.

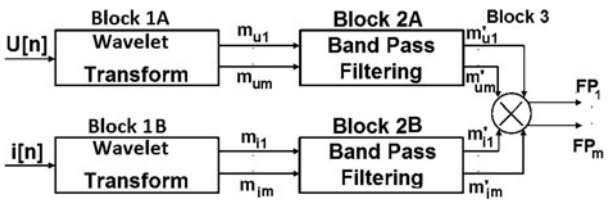

FIGURE 2. Block diagram of the proposed method.

4.1. WT—Blocks 1A/1B

WT has recently become well known as a useful tool in power system analysis that does not have fast Fourier transform (FFT) problems. If $x(t)$ is a time-varying signal, the continuous WT is defined as below [23]:

$$CWT(\tau, b) = |b|^{-\frac{1}{2}} \int_{-\infty}^{+\infty} x(t)\lambda^* \left(\frac{t-\tau}{b}\right) dt, \qquad (5)$$

where τ and b are translation and scale (Dilation) parameters, respectively. $\lambda^*(t)$ is the complex conjugate of the wavelet function $\lambda(t)$, which can be dilated through the control parameter of b and time shifted by the parameter of τ. Factor $|b|^{-\frac{1}{2}}$ is to ensure the energy preservation and normalization across the different scales. WT projects the original signal down onto basis functions and provides a mapping from the time domain to the time-scale plane. Wavelet function should satisfy the requirement of Eq. (6):

$$\int_{-\infty}^{+\infty} \lambda(t)dt = 0 \qquad (6)$$

such that the orthogonality can be guaranteed, which is critical in the wavelet paradigm. The orthogonality property indicates that the inner product of the base wavelet is unity with itself and zero with other scaled and shifted wavelets. As a result, an orthogonal wavelet is efficient for signal decomposition into non-overlapping sub-frequency bands.

To analyze various phenomena of the power network, different wavelet functions have been proposed (*e.g.*, Symlet, Mayer, and Daubechies). Feasibility of each basis function depends on the application requirements [24–26]. In this article, the modulated Gaussian wavelet was selected for frequency identification of modulated signals. By utilizing the Gaussian WT, it is of high flexibility in monitoring any frequency of interest in a waveform [27]. The Gaussian wavelet formulation is normalized exponential function-based and is symmetrical about $t = 0$. The symmetric property ensures that the base wavelet can serve as a linear phase filter [28]. The function also satisfies the requirement of Eq. (6).The Gaussian wavelet is a compact support wavelet, *i.e.*, the basis function is non-zero only within a finite interval. This allows the WTs to effectively represent signals that have localized features. The formulation of this function is given as follows:

$$\lambda(t) = \exp(j2\pi F_0 t - 0.5t^2), \qquad (7)$$

where F_0 is the central wavelet pulsation. In the study, F_0 has been selected to be 25π. Fourier transform (FT) of the

Gaussian function $\lambda(f)$ is another Gaussian with the central frequency of F_0. Each dilated wavelet will have a spread in the frequency domain equals to $\Delta\hat{\lambda}/b$ and a center frequency $\frac{F_0}{b}$. $\Delta\hat{\lambda}$ is the radius of $\lambda(f)$. A smaller value of $b$implies a higher resolution filter; *i.e.*, the signal is examined through a narrower WT window in a smaller scale. By adjusting the scale b, a series of different frequency components in the signal can be extracted. Note that the complex Gaussian WT was chosen as it provides the signal amplitude and phase angle simultaneously [29].

In this article, a discrete version of continuous WT will be used, which is expressed as follows:

$$CWT(b, iT_s) = T_s.\sum_{n=1}^{N_b} u(nT_s).\lambda^*\left[\frac{(n-i)T_s}{b} - \frac{N_{dw}.T_s}{2}\right], \tag{8}$$

where $u(nT_s)$ and $\lambda(nT_s)$ are the sampled versions of $u(t)$ and $\lambda(t)$, respectively. N_b is equal to $b \times N_{dw}$. If a signal is sampled at the interval of T_s for the duration of T_{ds}, the number of samples will be $N_{ds} = \frac{T_{ds}}{T_s}$, where sampling frequency is $f_s = \frac{1}{T_s}$. Now, if the wavelet function is sampled with the same sampling interval T_s, the duration will be equal to T_{dw} and $\mathrm{N_{dw}}=\frac{\mathrm{T_{dw}}}{\mathrm{T_s}}$, where N_{dw} is the total number of samples. In this study, it was assumed that $T_s = 0.001$ sec and $T_{dw} = 1024$ cycles. In the signal measurement, the sampling frequency and truncated window are often fixed. For such a scenario, $CWT(b, iT_s)$ can be practically deemed equal to $CWT(b)$ [27].

4.1.1. Signal Characteristics Determination by WT

The process of signal processing transforms a time domain signal into other domain since the characteristic information embedded within the time domain is not readily observable in its original form. Mathematically, this can be achieved by representing the time domain signal as a series of coefficients, based on a comparison between the signal $x(t)$ and template functions $\lambda_n(t)$:

$$C_n = \int_{-\infty}^{+\infty} x(t)\lambda_n^*(t)dt \tag{9}$$

Equation (9) shows the inner product of two functions. The inner product describes an operation of comparing the similarity between the signal and the template function, *i.e.*, the degree of closeness or correlation between the two functions. This is realized by observing the similarities between the WT and other commonly used techniques, in terms of the choice of the template functions. For example the FT is essentially a convolution between the time series $x(t)$ and a series of sine and cosine functions that can be viewed as template functions. The operation measures the similarity between $x(t)$ and the template functions, and expresses the average frequency information during the entire period of the signal.

WT is a tool that converts a signal into a different form. This conversion reveals the characteristics hidden in the original signal. In contrast to FT, the WT enables variable window sizes in analyzing different frequency components within a signal. Base wavelets are characterized by orthogonality, symmetry, and compact support. Understanding these properties will help choose a candidate base wavelet from the wavelet families for analyzing a special signal.

Through variations of the scale and time shifts of the base wavelet function, the WT can extract the components within over its entire spectrum. There are two quantitative concepts to determine optimal wavelet scale, which are maximum energy and correlation concepts.

4.1.1.1. Maximum energy.

The energy content of a signal $x(t)$ can be calculated by:

$$E = \int |x(t)|^2\, dt \tag{10}$$

It can also be calculated from its wavelet coefficients $WT(b, \tau)$ as

$$E = \int |WT(b, \tau)|^2\, dbd\tau \tag{11}$$

The above equation can be revised as

$$E(b) = \int |WT(b, \tau)|^2\, d\tau \tag{12}$$

Based on Parseval's theorem total energy contained in a waveform summed across all of time $t$is equal to the total energy of the waveform FT summed across all of its frequency components f. Therefore, if a major frequency component corresponding to a specific scaling b exists in the signal, then the wavelet coefficients at that scale will have relatively high magnitudes when this major frequency occurs. In fact, a base wavelet that can extract the largest amount of energy from the signal is desired. The energy related to that component can be extracted from the signal when applying WT with different scales. So, by varying the wavelet scale and determining the amplitude of WT versus scale, one can extract the frequency of interest from the main signal.

4.1.1.2. Correlation.

As mentioned, the inner product describes an operation of comparing the similarity between the signal and the template function, *i.e.*, the degree of closeness or correlation between the two functions.

The continuous WT (CWT) coefficients can be considered as a correlation coefficient and a measure of similitude between

the wavelet and the signal in the time scale plane. The higher the coefficient is, the more the similarity. In frequency domain, it means that if a major frequency component corresponding to a specific scaling b exists in the signal, then the wavelet coefficient at that scale will have relatively high magnitudes when this major frequency occurs. Therefore, by sweeping the frequency (varying scale), a wavelet scale b that which can maximize $CWT(b)$ is being sought.

4.1.2. Network Signal Characteristics Calculations

In the assessment of flicker frequency components a prerequisite procedure is to compute the system frequency. As mentioned, for any frequency of interest the wavelet amplitude around the frequency of interest should be computed by the sweeping the possible frequency range. A maximum of the wavelet coefficents corresponds with the frequency of interest. Now, for any frequency of interest, its corresponding wavelet amplitude B_k can be computed by the following equation:

$$B_k = \frac{(b_k)^{\frac{1}{2}} |CWT(b_k)|}{T_{dw}}. \tag{13}$$

First, the widest possible frequency range of the network frequency should be calculated. So, the values of b_k are computed by Eq. (13) for any values of k, where k is an integer whose maximum value is $\frac{(f_h - f_l)}{f_{ru}}$. f_h and f_l are the maximum and minimum of network frequency, and f_{ru} is the frequency resolution. Due to regular network frequency changes, $f_h = 50.5$ Hz, $f_l = 49.5$ Hz, and $f_{ru} = 0.01$ have been chosen ($k =$ 1 to 100);

$$b_k = \frac{F_0}{f_l + k f_{ru}}. \tag{14}$$

Second, by obtaining a set of different values of b_k, $CWT(b_k)$, and B_k can be calculated from Eqs. (8) and (10), respectively. After all B_k are computed, for the maximum B_k, its corresponding frequency f_b is the network frequency. Figure (3) shows B_k versus k for the typical signal of Figure 1. As expected, maximum of B_k is seen at $k(\max) = 50$ (corresponding to frequency of 50 Hz) and the value of B_k returns to zero on both sides of the maximum point.

Since complex wavelet function have been chosen, phase angle of the network signal can be computed from the following relationship:

$$\alpha = tg^{-1} \frac{\mathrm{Im}[CWT(b_{k(\max)})]}{\mathrm{Re}[CWT(b_{k(\max)})]}. \tag{15}$$

For determination of network signal amplitude one further step should be carried out. Now, B_k is computed again for a virtual signal with system frequency and known amplitude, *e.g.*, $\sqrt{2}\cos(2 * \pi * f_b t + \alpha)$. The computed B_k for virtual signal is, thus utilized for normalization. It compares with B_k of the actual network signal and the network signal amplitude is obtained.

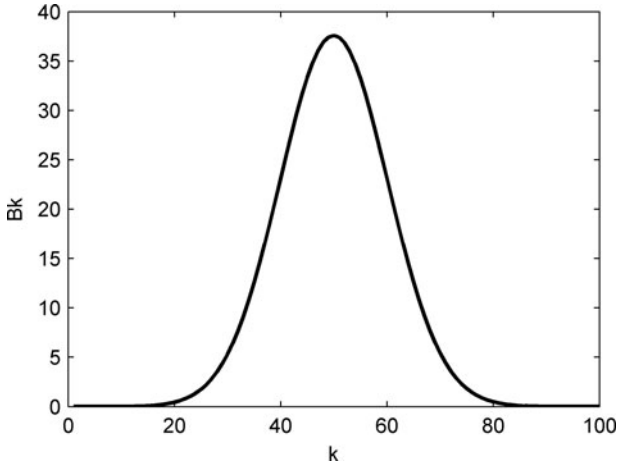

FIGURE 3. B_k versus k for network frequency determination.

4.1.3. Calculation of Flicker Components

After the system frequency was determined, the flicker components can be computed one by one. This is followed by the subtraction of the pure sinusoidal waveform with network frequency from the actual signal. The output will only contain the upper and lower frequency components ($f_b + f_m$ and $f_b - f_m$), which are non-overlapping sub-frequency bands (Eq. (4)). The next step is the separation of the individual flicker components. The WT can be used again for one of the subfrequency band at pleasure (*e.g.*, $f_b + f_m$). Similar to Eq. (11), the values of b_k should be first determined as follows:

$$b_k = \frac{F_0}{f_b + k f_{rf}}, \tag{16}$$

where f_{rf} is the flicker frequency resolution and was chosen as 0.1 Hz in this study. This means that $k$will start from 1 to 350 to cover fully the flicker frequency window from 0.5 to 35 Hz. After different values of b_k are calculated, Eq. (10) can be applied to compute the frequencies of the individual flicker components of the modulated signal. Figure (4) shows B_k versus k for the typical signal of Figure 1. As can be expected, two maximums of B_k are seen at $k = 100$ and $k = 200$ (frequency of 60 and 70 Hz) corresponding to flicker frequency of 10 and 20 Hz.

In the last step, the amplitude and phase angle of the flicker components should be obtained similar to the fundamental frequency.

4.2. Band-Pass Filter—Blocks 2A/2B

The flicker frequency signals are weighted according to how the human responds to flicker in blocks 2A/2B. The band-pass

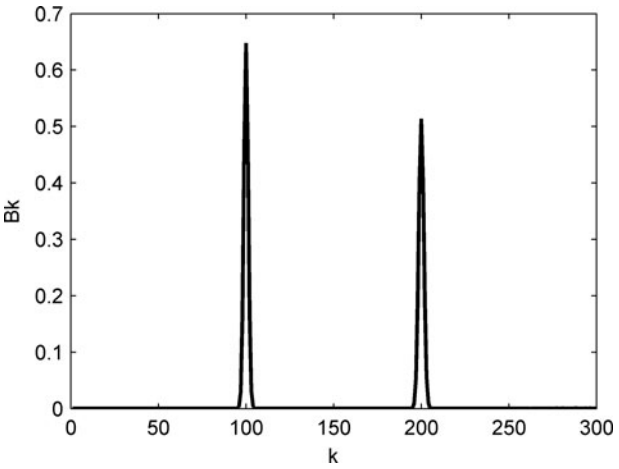

FIGURE 4. B_k versus k for flicker frequency determination.

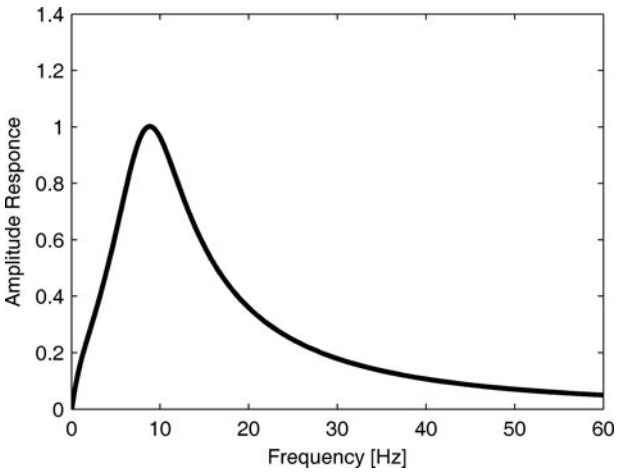

FIGURE 5. Frequency response of band-pass filter.

filter provided in these blocks is identical to digital band-pass filter defined in IEC 61000-4-15. The standard applies the human sensitivity curve on flicker signal. The transfer function of the IEC standard filter is

$$F(s) = \frac{k\omega_1 s}{s^2 + 2\lambda s + \omega_1^2} \times \frac{1 + s/\omega_2}{\left(1 + \frac{s}{\omega_3}\right)\left(1 + \frac{s}{\omega_4}\right)} \qquad (17)$$

The parameters of Eq. (17) for a light with rated values of 60 W/230 V are shown in Table 1. The frequency response of the IEC filter is shown in Figure 5. As it can be seen, it peaks at the frequency 8.8 Hz. The attenuation of the filter matches with the human eye sensitivity curve presented in the standard.

4.3. FPs of Flicker Frequency Components—Block 3

The FPs are computed in block 3 for all extracted flicker frequencies by product of voltage and current flicker amplitude with the same frequency and phase angle between them. Mathematically we have:

$$FP = \frac{1}{2}\sum_m U_m I_m \cos(\alpha_{mv} - \alpha_{mi}) \qquad (18)$$

where $\frac{U_m}{\sqrt{2}}(\frac{I_m}{\sqrt{2}})$ and $\alpha_{mv}(\alpha_{mi})$ are the amplitudes and phase angle of voltage (current) flicker.

$k = 1.74802$	$\lambda = 2\pi \times 4.05981$
$\omega_1 = 2\pi \times 9.15494$	$\omega_3 = 2\pi \times 1.22535$
$\omega_2 = 2\pi \times 2.27979$	$\omega_4 = 2\pi \times 21.9$

TABLE 1. Filter coefficients for the transfer function (Eq. (14))

5. SIMULATION RESULTS

To examine the accuracy of the proposed method, the IEEE 13-bus system is simulated in MATLAB/Simulink (The MathWorks, Natick, Massachusetts, USA). The test network is shown in Figure 6. For the simulations two different cases are considered. First, it is assumed there is only a single flicker source (130 kW) at bus 633. Second, the network has been considered with two identical flicker sources at buses 633 and 680. The FPs are computed in the measuring (monitoring) points a, b, c, d, and e as shown in Figure 6. The results are presented in the following text. To assess the performance of the proposed algorithm, a comparison with the method of [16] has been presented.

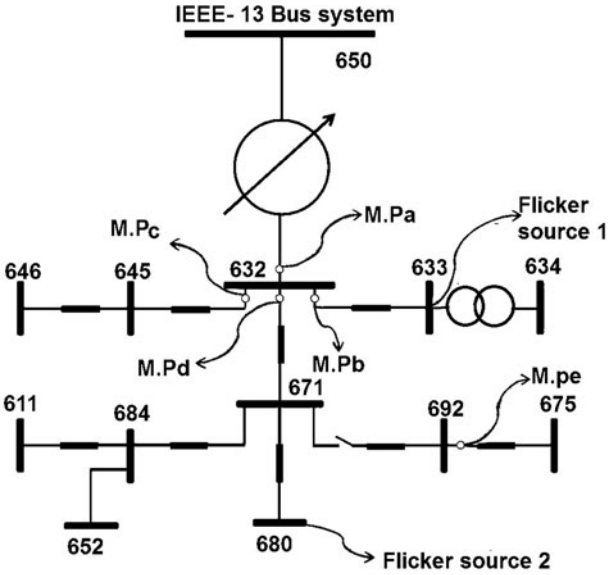

FIGURE 6. Single-line diagram for IEEE 13-bus test system.

Monitoring point *e*	Monitoring point *d*	Monitoring point *c*	Monitoring point *b*	Monitoring point *a*	Methods
0.0491	0.0589	0.1021	–4.969	–4.0806	Method presented in [15]
0.0900	0.0998	0.1335	–5.5044	–4.9028	Proposed method

TABLE 2. Simulation results for Case 1

5.1. Case 1: Single Flicker Source

In this case, it is assumed there is only one flicker source at bus 633. The frequency and depth of the flicker source are 10 Hz and 7%, respectively. The flicker source is located below the measuring points a and b as shown in Figure 6. Then, negative FPs are expected at these points. The other measuring points are located downstream with respect to the flicker source. The sign of the FPs is, therefore, expected to be positive. On the other hand, the measuring points b and e are the closest and the farthest points to the flicker source, and the magnitude of FPs at these points should thus, be the biggest and smallest values, respectively. From the above discussion, validating simulation has been performed and FPs were computed in the monitoring points. Simulation results are shown in Table 2. As it is seen, sign and magnitude of the FPs are exactly as expected.

5.2. Case 2: Multiple Flicker Sources

In this case two flicker sources are assumed in the test network. The first is connected to bus 633 with flicker frequency and modulation depth of 10 Hz and 7%, respectively. The second flicker source is located at bus 680 with flicker frequency of 20 Hz. The modulation depth of this flicker source is also assumed 7%. Locations of the monitoring points are the same as Case 1. Simulation was performed and the results have been shown in Table 3. For each monitoring point, the following discussions can be conducted.

5.2.1. Monitoring Point a

The proposed method gives two negative FPs at flicker frequencies of 10 and 20 Hz and the magnitude of the FP at 10-Hz flicker frequency is much bigger than the one at 20 Hz. Signs of the FPs show that there is no contribution from the high voltage (utility) to the low voltage network. The results also indicate two scenarios for this situation.

1. Scenario 1: There are two flicker sources in one of the branches that are connected to bus 632 and the flicker source with 10-Hz flicker frequency is the dominant one.
2. Scenario 2: There are two flicker sources in separate branches that are linked to bus 632. Both of them are downstream with respect to monitoring point a. The flicker source with the flicker frequency of 20 Hz is at the greater distance with respect to the measuring point. In the other words, the flicker source 1 has more contribution to the flicker level than the flicker source 2 (flicker source 1 is the dominant flicker source for this monitoring point).

The previous methods within this topic give just a single value for FP at a monitoring point. Therefore, the methods are not able to identify the other flicker sources in the network.

5.2.2. Monitoring Point b

In this measuring point, sign of the 20-Hz FP is positive, whereas the 10-Hz FP is negative. The 10-Hz flicker source is, therefore, located downstream and the 20-Hz flicker source is located upstream with respect to the monitoring point b. This indicates that scenario 2 should be the correct scenario.

5.2.3. Monitoring Point c

The calculated FPs are positive at this point. Both of the flicker sources are thus located upstream with respect to this measuring point and the branch has no contribution to the flicker level of bus 632.

Monitoring point *a*	Monitoring point *b*	Monitoring point *c*	Monitoring point *d*	Monitoring point *e*		
0.100	−0.195	0.107	−5.057	−5.294	Method presented in [15]	
0.070	0.079	0.132	−5.497	−4.983	$f_{m1} = 10$	Proposed method
0.068	−0.325	0.026	0.005	−0.744	$f_{m2} = 20$	
0.138	−0.246	0.159	−5.492	−5.727	Total	

TABLE 3. Simulation results for Case 2

5.2.4. Monitoring Point d

Due to the upstream 20-Hz flicker source, sign of the 20-Hz FP is negative. The total FP is also negative in this monitoring point. However, the voltage of bus 632 has been polluted by the 10-Hz flicker source, but it can be supposed that a large amount of the flicker generated by this flicker source flows to the main source of the network and only a small portion of that flows downstream.

5.2.5. Monitoring Point e

The sign of the FPs are positive. Both flicker sources are, therefore, located upstream with respect to this measuring point. The 10-Hz flicker source is at the greater distance to this monitoring point, but the magnitudes of the 10- and 20-Hz FPs are approximately equal. Note that both flicker sources have equal amplitude, but flicker with frequency of 10 Hz has higher sensitivity coefficient than 20-Hz flicker according to IEC standard. In fact, two flicker sources are located at the same *equivalent distance* from the monitoring point e. For calculating the equivalent distance of a flicker source from a busbar, three parameters should be considered: flicker frequency, modulating depth, and the distance (impedance) between the flicker source and the busbar.

6. CONCLUSION

The article presented a new method based on WT and FP theory to identify the individual flicker sources in a multi-FP grid. The key ideas of the method are finding out the FP at each flicker frequency component and defining the FP as a quantity containing both the sign and the magnitude. The demodulation process is achieved by a discrete version of a continuous wavelet function called modulated Gaussian wavelet. By utilizing the Gaussian WT, it is of high flexibility in monitoring any frequency of interest in a waveform. For any frequency of interest the wavelet amplitude around the frequency of interest was computed by the sweeping the possible frequency range. The maximum of the wavelet coefficents shows the frequency of interest. Complex Gaussian WT was chosen as it provides the signal amplitude and phase angle simultaneously. After the system frequency was determined, the flicker components amplitudes and phase angles computed one by one. The flicker frequency signals are then weighted according to how the human responds. Finally, the FPs were computed for all extracted flicker frequencies by product of voltage and current flicker amplitude with the same frequency and phase angle between them. The main characteristics of the method follow.

- Both amplitudes and phase angles of flicker components are computed by the chosen complex wavelet function. The undesired and additional low-frequency components in flicker frequency window are eliminated.
- The method is able to easily calculate the FP from the amplitudes and phase angles of flicker components.
- The method is such that the superposition principle can be applied to FP.
- The method can identify the number and locations of flicker sources in a multi-flicker source power network.
- The method provides the possibility of the separation of the flicker effect of the individual consumers connected to the same busbar. In fact, the branch contribution to the busbar flicker level can be determined which helps to reduce challenging between the utility and consumers and speeds up the mitigation process.
- The method can be simply implemented on existing digital meters.

The article also introduced a new parameter called "flicker equivalent distance."

REFERENCES

[1] Halpin, M., Cai, R., and Yang, X., "A review of flicker objectives related to complaints, measurements, and analysis techniques," *20th International Conference on Electricity Distribution (CIRED 2009)*, paper 0755, Prague, 8–11 June 2009.

[2] Mendis, S., Bishop, M., and Witte, J., "Investigations of voltage flicker in electric arc furnace power systems," *IEEE Ind. Appl. Mag.*, Vol. 2, No. 1, pp. 28–34, 1996.

[3] Moallem, P., Zargari, A., and Kiyoumarsi, A., "A practical framework for applying effects of various lamps on IEC flickermeter and evaluating results in a welding system," *Electr. Power Compon. Syst.*, Vol. 27, No. 7, pp. 1047–1054, 2011.

[4] Hong, Y. Y., and Wang, J. J., "Calculation of voltage fluctuation cased by intermittent loads," *Electr. Power Compon. Syst.*, Vol. 35, No. 4, pp. 421–429, 2012.

[5] Larsson, Å., "Flicker emission of wind turbines during continuous operation," *IEEE Trans. Energy Conver.*, Vol. 17, pp. 114–118, 2002.

[6] Tande, J., and Uhlen, K., "Wind turbines in weak grids—Constraints and solutions," *16th International Conference on Electricity Distribution (CIRED 2001)*, 18–21 June 2001.

[7] IEC, "Flicker meter—functional and design specifications," *IEC Standard* 61000-4-15, 2010.

[8] Afshar, F. G., "Light flicker factor as a diagnostic quantity for the evaluation of discharge instabilities in HID lamps," *Electr. Power Compon. Syst.*, Vol. 3, No. 1, pp. 35–50, 2006.

[9] Srinivasan, K., "RMS fluctuations attributable to a single customer," *Power Quality Solutions*, *Proc. B.*, Vol. 8, pp. 68–71, 1995.

[10] Dan, A., "Identification of flicker sources," *International Conference on Harmonics and Quality of Power*, Athens, Greece, 14–16 October 1998.

[11] Hughes, B., "Source identification for voltage sag and flicker," *IEEE Power Engineering Society Summer Meeting*, Seattle, WA, 1–4 May 2000.
[12] Egtedarpour, N., and Farjah, E., "Intelligent identification of flicker source in distribution system," *IET Generat. Transm. Distribut.*, Vol. 4, No. 9, pp. 1016–1027, 2010.
[13] Simoes, M., and Deckmann, S., "Flicker propagation and attenuation," *8th International Conference on Harmonics and Quality of Power*, Athens, Greece, 14–16 October 1998.
[14] Zhang, D., Xu, W., and Nassif, A., "Flicker source identification by interharmonic power direction," *IEEE Canadian Conference on Computer Engineering*, Saskatoon, Saskatchewan, Canada, 1–4 May 2005.
[15] Hernandez, A., Mayordomo, J., Asensi, R., and Beites, L., "A method based on inter-harmonics for flicker propagation applied to arc furnaces," *IEEE Trans. Power Deliv.*, Vol. 20, pp. 2334–2342, 2005.
[16] Axelberg, P. G. V., and Bollen, M. H. J., "An algorithm for determining the direction to a flicker source," *IEEE Trans. Power Deliv.*, Vol. 21, No. 2, pp. 755–760, 2006.
[17] Peter, G. V., Axelberg, M., Bollen, H. J., "Trace of flicker sources by using the quantity of flicker power" *IEEE Trans. Power Deliv.*, Vol. 23, No. 1, pp. 465–471, 2008.
[18] Poormonfaredazimi, M., Moghadam, H., Doroudi, A., "A novel method to trace flicker sources," *17th Electric Power Distribution Conference (PDC)*, Tehran, Iran, 2–3 May 2008.
[19] Angrisani, L., Daponte, P., and Testa, A., "A measurement method based on the wavelet transform for power quality analysis," *IEEE Trans. Power Deliv.*, Vol. 13, No. 4, pp. 990–998, 1998.
[20] Hasheminejad, S., Esmaeili, S., and Jazebi, S., "Power quality disturbance classification using S-transform and hidden Markov model," *Electr. Power Compon. Sys*., Vol. 40, pp. 1160–1182, 2012.
[21] Chang, W. N., and Wu, C. J., "A flexible voltage flicker teaching facility for electric power quality education," *IEEE Trans. Power Syst.*, Vol. 13, No. 1, pp. 27–33, 1998.
[22] Poisson, O., Riuual, P., and Meunier, M., "New signal processing tools applied to power quality analysis," *IEEE Trans. Power Deliv.*, Vol. 14, pp. 561–566, 1999.
[23] Strang, G., and Nguyen, T., *Wavelets and Filter Banks*, Cambridge, MA: Wellesley-Cambridge, Chap. 7, 1997.
[24] Nicolae, I.-D., "Using discrete wavelet transform to evaluate power quality at highly distorted three-phase systems," *11th International Conference on Electrical Power Quality and Utilization (EPQU),* Lisbon, Portugal, 17–19, October 2011.
[25] Jinfeng, R., "Real-time power system frequency and phasor estimation using recursive wavelet transform," *IEEE Trans. Power Deliv.*, Vol. 26, No. 3, pp. 1392–1402, July 2011.
[26] Dwivedi, U. D., and Singh, S. N., "A wavelet-based de-noising technique for improved monitoring and characterization of power quality disturbances," *Electr. Power Compon. Syst.*, Vol. 37, No. 7, pp. 753–769, 2009.
[27] Huang, S., and Lu, C., "Enhancement of digital equivalent voltage flicker measurement via continuous wavelet transform," *IEEE Trans. Power Deliv.*, Vol. 19, No. 2, pp. 663–670, 2004.
[28] Zhang, X. P., and Peng, Y. N., "Orthogonal complex filter banks and wavelets: Some properties and design," *IEEE Trans. Signal Process.*, Vol. 47, No. 4, pp. 1039–1048, 1999.
[29] Torrence, C., and Compo, G. P., "A practical guide to wavelet analysis," *Bull. Amer. Meteor. Soc.*, Vol. 79, pp. 61–78, 1998.

BIOGRAPHIES

Hadi Moghadam Banayem was born in 1984 in East Azerbaijan, Iran. He received his B.Sc. in electrical engineering from the Azad University of Tabriz, Tabriz, Iran, in 2007, and his M.Sc. in electrical engineering from the Shahed University, Tehran, Iran, in 2011. He is currently a Ph.D student in the Electrical Engineering Department, Urmia University, West Azerbaijan, Iran. His special field of interest includes power quality.

Aref Doroudi was born in 1968 in Tehran, Iran. He received his B.Sc. from the Electrical Engineering Department of Amirkabir University of Technology, Tehran, Iran, in 1992; his M.S. in electrical engineering from the Tabriz University, Tabriz, Iran, in 1994; and his Ph.D. in electrical engineering from Amirkabir University of Technology, Tehran, Iran, in 2000. Currently, he is an assistant professor in the Electrical Engineering Department, Shahed University, Tehran, Iran. His special fields of interest include power quality, electric machine design, and power systems dynamics.

Mohammad Poormonfared Azimi was born in 1988 in Tehran, Iran. He received the B.Sc. from the Electrical Engineering Department of Shahed University, Tehran, Iran, in 2010, and his M.Sc. in electrical engineering from the Shahed University, Tehran, Iran, in 2012. His special fields of interest include renewable energy and power quality.